Vortex Paradigm for Shock-Accelerated Density-Stratified Interfaces

John F. Hawley
Institute for Theoretical Physics, University of California, Santa Barbara, Santa Barbara, California 93106
and Department of Astronomy, University of Virginia, P.O. Box 3818, Charlottesville, Virginia 22903

Norman J. Zabusky
Institute for Theoretical Physics, University of California, Santa Barbara, Santa Barbara, California 93106
and Department of Mechanical and Aeronautical Engineering, Rutgers University, P.O. Box 909, Piscataway, New Jersey 08855
(Received 27 March 1989)

We present a vortex paradigm for interpreting the evolution of shock-accelerated density-stratified interfaces beyond early times. The paradigm is investigated and illustrated through a series of numerical experiments that compare favorably with recent shock-tube experiments. Color images of space-time diagrams of the one-space integrated vorticity function highlight primary and secondary features of the emerging vortex structures.

PACS numbers: 47.40.Nm, 47.20.−k

The evolution of shock-accelerated density-stratified interfaces is of considerable fundamental and practical interest. Laboratory experiments[1-5] have been performed with both unperturbed and perturbed planar interfaces, and recently Haas and Sturtevant[6] have done careful experiments in which shocks accelerate cylindrical and spherical bubbles. These laboratory results have stimulated several numerical investigations.[7-10] In the present study, we shall consider the shock to enter from the left through a medium of density ρ_1, striking an interface (contact surface) that separates a region of density ρ_2 with $\eta=\rho_2/\rho_1$. The laboratory and numerical results of such experiments are often interpreted quantitatively via the linear instability analysis of Richtmyer which is an extension of the Rayleigh-Taylor instability.[11] This linear analysis finds that the configurations are "stable" if $\eta<1$ and "unstable" if $\eta>1$. (It is convenient to speak of $\eta<1$ as a "slow-fast" interface and $\eta>1$ as a "fast-slow" interface.[12])

This stability designation is physically (and observationally) *misleading* in the sense that perturbations to planar interfaces for any η can evolve substantially away from their initial configurations after a very short time (i.e., the linear epoch is very short). Sturtevant[1] notes this poor comparison between experimentally determined growth rates and linear theory calculations.

In the present paper, we show that more physical insight can be gained from a vortex deposition-evolution (or emergent coherent structure) viewpoint. The role of vorticity deposition was emphasized in previous shock-bubble simulations.[8-10] However, the shock-bubble geometry is complicated because of the strong coupling among many competing processes. Furthermore, the simulations of Picone and Boris[8] are marginally resolved, and the circulation-generation formula is not generally applicable. Winkler *et al.*[9] and Chalmers *et al.*[10] describe higher-resolution simulations that discover new morphologies, but they provide insufficient diagnostic and interpretative information.

We now report on appropriately resolved numerical simulations that capture the essential features and space-time scales observed by Haas and Sturtevant[13] when a planar shock accelerates an inclined planar interface between two media (Fig. 1). The numerical results can be compared with the laboratory results, displayed as the usual shadowgraphs that manifest the second spatial derivative of density. Unfortunately, this traditional way of exhibiting results tends to obscure a vortex-dynamical interpretation. The detailed diagnostics available to a numerical simulation have no such limitation. Our calculations are performed in a *simple* two-dimensional Cartesian geometry with a time-explicit, Eulerian finite-difference code. The code uses a monotonic advection scheme by van Leer,[14] and a scalar artificial viscosity for shock resolution. The simulations presented here were obtained on an 800×128 (x,y) grid with equal spacing in x and y. Further discussion of the code, and of extensive code validation tests, is postponed to a future publication.

Figure 1 shows the density evolution for two of the numerical experiments in which the interface is inclined at an angle of 60° to the incoming Mach 1.2 shock. In Fig. 1(a) $\eta=0.14$ (slow-fast case, e.g., air-helium), and in Fig. 1(b) $\eta=3.0$ (fast-slow case, e.g., air-freon). Both fluids are modeled as simple $\gamma=1.4$ ideal gases. We adopt units in which the isothermal sound speed in air, $c_{\rm iso}^2=p/\rho$, is unity. Two advanced times (t_1 and t_2) are shown in each figure, with the initial location of the shock and contact surface shown as vertical and inclined dashed lines ($t=0$) on the t_1 frame. The time t_1 is selected when the shock has just traversed the initial interface. The time t_2 is a late time chosen for comparison with Sturtevant's experiment.[1,13] An excellent overview of the competing vortex processes is obtained by examin-

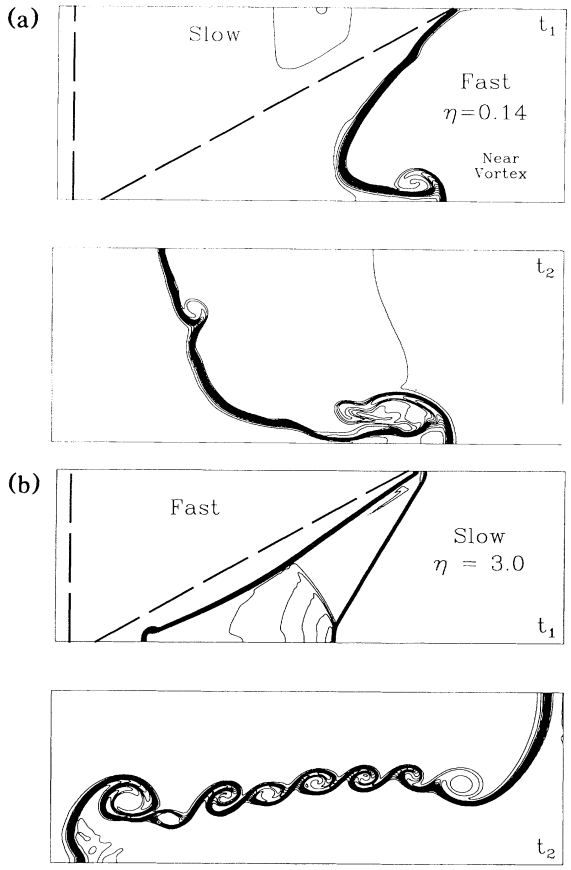

FIG. 1. (a) Density contours for the slow-fast $M=1.2$, $\eta=0.14$ interface evolution at two times, $t_{1a}=107$ and $t_{2a}=213$. In the upper (lower) figure the x range is 0–160 (100–260), and the y range is 0–62. The dashed lines indicate the initial shock and contact discontinuity locations. (b) Density contours for the fast-slow $M=1.2$, $\eta=3.0$ interface evolution at two times, $t_{1b}=91$ and $t_{2b}=620$. In the upper (lower) figure the x range is 0–180 (135–315), and the y range is 0–62. The dashed lines indicate the initial shock and contact discontinuity locations.

ing space-time diagrams of y-integrated vorticity [$\gamma(x,t)=\int_0^{y\max}\omega(x,y,t)dy$; Fig. 2]. We now examine the slow-fast and fast-slow cases in turn.

As the shock traverses the interface it generates vorticity (mostly positive for $\eta<1$, and mostly negative for $\eta>1$). Thus, the first phase of the evolution can be thought of as *vorticity deposition*. The instantaneous angular displacement of the interface, and the circulation deposited along it, can be obtained from a shock-polar analysis[12,15,16] for a reasonable set of parameters: η, the angle of the interface, and the shock strength or Mach number. For a sufficiently simple shock-contact interaction (as for the fast-slow case), the total circulation is obtained with high accuracy. After the shock has passed the interface, the essential feature is an angularly displaced, translating contact surface which bears a thin layer of vorticity (since the transitional region occupies a few zones). Thus begins the *vorticity evolution* phase. The vortex layer diffuses laterally (due to numerical diffusion) as it rotates globally. The ends of the vortex layer begin to roll up. As seen in Fig. 1(a), the roll up of the lower interface region (near vortex) proceeds as the vorticity "binds" with its mirror image. This is the dominant mechanism for the formation of the "wall vortex." This bound vortex becomes the "wall jet" seen in experiments.[1,13] The upper-lower asymmetry in the vortex roll up is due at least in part to the shock wave that is reflected from the contact surface as it is again reflected back into the region by the upper boundary. These secondary processes will be discussed in detail elsewhere. Note that the density interface perturbations in the last frame of Fig. 1(a) are consistent with the layer's instability. Figure 9(a) in Sturtevant's book[1] shows perturbations on the density interface similar to those seen behind the wall vortex in Fig. 1(a). These are more clearly visible in the unpublished work of Haas and Sturtevant.[13]

In the space-time diagram [Fig. 2(a)] we obtain insight into magnitudes and rates of change of the vorticity. We label several features: (1) A line that gives the transmitted shock speed through region 2; (2) the incident shock speed in region 1; (3) the left-most end of the interface; (4) the emerging dipolar (or bound) vortex on the lower boundary; (5) the rotated, nearly vertical interface occupying most of the vertical extent; and (6) the space-time trajectory of the dominant wall vortex.

We now discuss the evolution of the fast-slow density layer pictured in Fig. 1(b) where $M=1.2$ and $\eta=3.0$. Note, however, that the magnitude of the density ratio is less than that in the slow-fast case, and the interface has acquired less circulation. By direct numerical integration we can monitor the total circulation present on the grid as a function of time. At time t_{1a} the slow-fast interaction has a total circulation $\Gamma=\int\omega\,dx\,dy=64$, whereas at t_{1b} the fast-slow circulation has a value $\Gamma=-25$ (an idealized shock-polar analysis, neglecting the shock reflected off the wall at $y=0$ predicts $\Gamma=-23$). The negative vorticity causes the interface to rotate globally in the *opposite* direction, namely, away from the wall. There is a slight left-to-right asymmetry. In Fig. 2(b) we see the following: (1) the incident shock traversing the contact discontinuity; (2) the width in x of the interface at t_{1b}; (3) the larger width in x of the interface at t_{2b} due to the net effect of the lower (upper) edge dipoles moving upstream (downstream) relative to the ambient flow; (4) the left (or lower) vortex initially moving more slowly than the right (or upper) vortex (5) because of the motion of the dipolar bound vortices relative to the mean post-shock flow; (6) the nascent emergence of the rolled-up interface due to the instability of the vortex layer; and (7) a merger, and another merger in

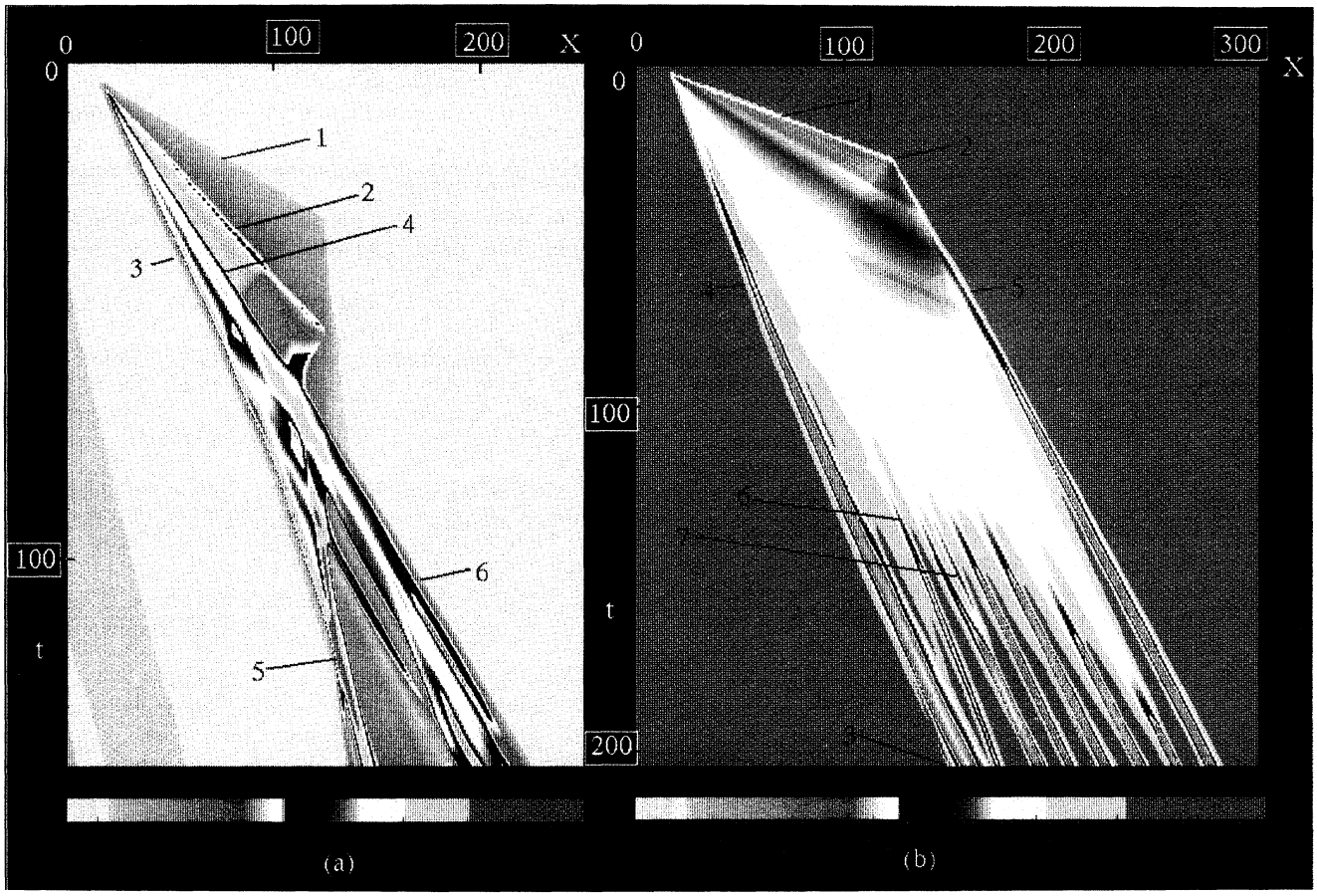

FIG. 2. (a) Color image of the space-time diagram of y-integrated vorticity $\gamma(x,t)$ for the slow-fast interaction $M=1.2$, $\eta=0.14$. The color map is chosen so that low (high) values are blue (red), and the logarithmic scale was obtained by rendering the function $a\sinh(\gamma)$. The time axis is labeled by frame number; each frame corresponds to 1.5 time units, defined so that the isothermal sound speed equals one. The sharp white-black transition highlights the wall vortex at 6 and the complex structure following indicates a merger event with a weaker trailing vortex. Label numbers indicate specific events described in the text. (b) Color image of the space-time diagram of y-integrated vorticity $\gamma(x,t)$ for the fast-slow interaction $M=1.2$, $\eta=3.0$. The color map renders a linear vorticity scale and the sharp white-black transition highlights the emerging vortex structures. The time axis is labeled by frame number; each frame corresponds to 3.0 time units, defined so that the isothermal sound speed equals one. The large yellow field indicates a near-uniform vortex layer which is transforming into eight rolled-up (blue) vortex centers. Label numbers indicate specific events described in the text.

progress near (3). The vorticity at about time 200 (not shown) reveals the eight vortex centers seen in Fig. 1(b). The number of vortex centers is a function of the thickness of the vortex layer (which depends upon numerical resolution and diffusion), scale of the perturbation, etc.

In conclusion, we have shown that a deeper and broader physical understanding of shock-accelerated density-stratified interfaces is obtained by considering vorticity deposition and emergence of coherent vortex structures. The total circulation and the local interface position at t_1 are accurately given by a shock-polar analysis. Furthermore, for the slow-fast interface [Fig. 1(a)], we observe in both the laboratory and numerical experiments that the roll up at the upper edge is weaker. This broken symmetry results from secondary shocks and baroclinic effects. The longer time evolution of the dominant vortex is understood best through a mechanism of binding with mirror images. (However, when a strong wall vortex forms, experiments show an enhanced movement away from the wall. This may be a boundary-layer phenomenon, which is not simulated by the present code.) Another striking laboratory-numerical similarity are the growing undulations along the stretching interface layer. Thus, small and physically important scales have been captured by this Eulerian code. The simple geometry studied in this paper helps us easily interpret

observed phenomena and previews the complexity of interacting processes in more practical geometries, as will be discussed in future publications.

Finally, we conjecture that our vorticity deposition-evolution paradigm is generic to a class of interface problems. In other physical media (e.g., plasma and magnetohydrodynamic), different sources of the flow (e.g., currents, or monopolar or dipolar charges) will concentrate near the excited interface, and these sources will govern the flow on longer time scales.

N.J.Z. acknowledges instructive communications with J.-F. Haas, B. Sturtevant (who kindly provided his unpublished experimental data), and J. Grove. P. Colella provided information on other numerical and experimental work in progress. N.J.Z. acknowledges partial support from the Naval Research Laboratory under Contract No. N00014-86-C-2336 and the NSF. J.F.H. acknowledges support from NSF Grant No. PHY88-02747 and NASA Grant No. NAGW-1510. This work was begun while both authors were at the Institute for Theoretical Physics, supported by NSF Grant No. PHY82-17853, supplemented by funds from NASA. Supercomputer calculations were carried out on the National Center for Supercomputing Applications Cray 2.

[1]B. Sturtevant, in *Shock Tubes and Waves,* edited by H. Grönig (VCH Verlag, Berlin, 1987), p. 89.

[2]E. E. Meshkov, Sov. Fluid Dyn. **4**, No. 5, 101 (1969).

[3]V. A. Andronov, S. M. Bakhrakh, E. E. Meshkov, V. N. Mokhov, V. V. Nikiforov, A. V. Pevnitskii, and A. I. Tolshmyakov, Zh. Eksp. Teor. Fiz. **71**, 806 (1976) [Sov. Phys. JETP **44**, 424 (1976)].

[4]R. F. Benjamin, H. E. Trease, and J. W. Shaner, Phys. Fluids **27**, 2390 (1984).

[5]S. G. Zaitsev, E. V. Lazareva, V. V. Chernukha, and V. M. Belyaev, Dokl. Akad. Nauk SSR **283**, 94 (1985) [Sov. Phys. Dokl. **30**, 579 (1985)].

[6]J.-F. Haas and B. Sturtevant, J. Fluid Mech. **181**, 41 (1987).

[7]D. L. Youngs, Physica (Amsterdam) **12D**, 32 (1984).

[8]J. M. Picone and J. P. Boris, J. Fluid Mech. **189**, 23 (1988).

[9]K.-H. A. Winkler, J. W. Chalmers, S. W. Hodson, P. R. Woodward, and N. J. Zabusky, Phys. Today **40**, No. 10, 28 (1987).

[10]J. W. Chalmers, S. W. Hodson, K.-H. A. Winkler, P. R. Woodward, and N. J. Zabusky, Fluid Dyn. Res. **3**, 392 (1988).

[11]R. D. Richtmyer, Commun. Pure Appl. Math. **8**, 297 (1980).

[12]L. Henderson, J. Fluid Mech. **26**, 607 (1966).

[13]J.-F. Haas and B. Sturtevant, Caltech report, 1985 (unpublished).

[14]B. van Leer, J. Comput. Phys. **23**, 276 (1977).

[15]R. Courant and K. O. Friedrichs, *Supersonic Flow and Shock Waves,* (Springer-Verlag, New York, 1948), pp. 294–317.

[16]J. Grove, Adv. Appl. Mech. (to be published).

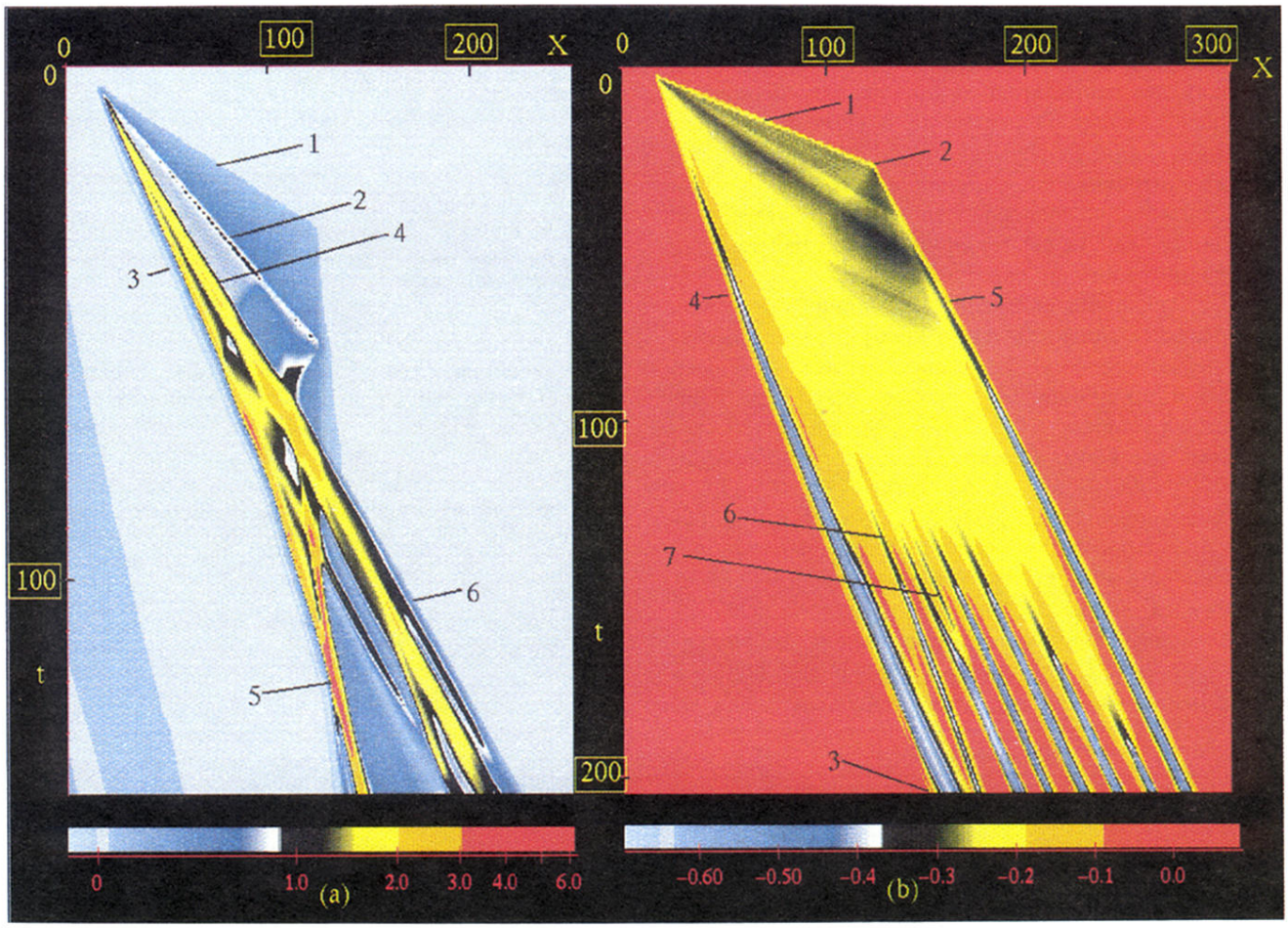

FIG. 2. (a) Color image of the space-time diagram of y-integrated vorticity $\gamma(x,t)$ for the slow-fast interaction $M=1.2$, $\eta=0.14$. The color map is chosen so that low (high) values are blue (red), and the logarithmic scale was obtained by rendering the function $a\sinh(\gamma)$. The time axis is labeled by frame number; each frame corresponds to 1.5 time units, defined so that the isothermal sound speed equals one. The sharp white-black transition highlights the wall vortex at 6 and the complex structure following indicates a merger event with a weaker trailing vortex. Label numbers indicate specific events described in the text. (b) Color image of the space-time diagram of y-integrated vorticity $\gamma(x,t)$ for the fast-slow interaction $M=1.2$, $\eta=3.0$. The color map renders a linear vorticity scale and the sharp white-black transition highlights the emerging vortex structures. The time axis is labeled by frame number; each frame corresponds to 3.0 time units, defined so that the isothermal sound speed equals one. The large yellow field indicates a near-uniform vortex layer which is transforming into eight rolled-up (blue) vortex centers. Label numbers indicate specific events described in the text.